JACS
JOURNAL OF THE AMERICAN CHEMICAL SOCIETY
Article
pubs.acs.org/JACS

Thermal Structural Transitions and Carbon Dioxide Adsorption Properties of Zeolitic Imidazolate Framework-7 (ZIF-7)

Wanxi Cai,[†] Taehee Lee,[†] Maro Lee,[‡] Woosuk Cho,[§] Doug-Young Han,[∥] Nakwon Choi,[⊥] Alex C. K. Yip,[#] and Jungkyu Choi*[,†,▽]

[†]Department of Chemical & Biological Engineering, College of Engineering, Korea University, Anam-dong, Seongbuk-gu, Seoul 136-713, Republic of Korea

[‡]Department of Chemical Engineering, Soongsil University, Sangdo-dong, Dongjak-gu, Seoul 156-743, Republic of Korea

[§]Advanced Batteries Research Center, Korea Electronics Technology Institute (KETI), #68 Yatap-dong, Bundang-gu, Seongnam, Gyeonggi 463-816, Republic of Korea

[∥]Seoul Center, Korea Basic Science Institute, Anam-dong, Seongbuk-gu, Seoul 136-713, Republic of Korea

[⊥]Center for BioMicrosystems, Brain Science Institute, Korea Institute of Science and Technology (KIST), Seoul 136-791, Republic of Korea

[#]Department of Chemical and Process Engineering, University of Canterbury, Ilam, Christchurch, New Zealand

[▽]Green School, Korea University, Anam-dong, Seongbuk-gu, Seoul 136-713, Republic of Korea

Supporting Information

ABSTRACT: As a subset of the metal−organic frameworks, zeolitic imidazolate frameworks (ZIFs) have potential use in practical separations as a result of flexible yet reliable control over their pore sizes along with their chemical and thermal stabilities. Among many ZIF materials, we explored the effect of thermal treatments on the ZIF-7 structure, known for its promising characteristics toward H_2 separations; the pore sizes of ZIF-7 (0.29 nm) are desirable for molecular sieving, favoring H_2 (0.289 nm) over CO_2 (0.33 nm). Although thermogravimetric analysis indicated that ZIF-7 is thermally stabile up to ∼400 °C, the structural transition of ZIF-7 to an intermediate phase (as indicated by X-ray analysis) was observed under air as guest molecules were removed. The transition was further continued at higher temperatures, eventually leading toward the zinc oxide phase. Three types of ZIF-7 with differing shapes and sizes (∼100 nm spherical, ∼400 nm rhombic-dodecahedral, and ∼1300 nm rod-shaped) were employed to elucidate (1) thermal structural transitions while considering kinetically relevant processes and (2) discrepancies in the N_2 physisorption and CO_2 adsorption isotherms. The largest rod-shaped ZIF-7 particles showed a delayed thermal structural transition toward the stable zinc oxide phase. The CO_2 adsorption behaviors of the three ZIF-7s, despite their identical crystal structures, suggested minute differences in the pore structures; in particular, the smaller spherical ZIF-7 particles provided reversible CO_2 adsorption isotherms at ∼30−75 °C, a typical temperature range of flue gases from coal-fired power plants, in contrast to the larger rhombic-dodecahedral and rod-shaped ZIF-7 particles, which exhibited hysteretic CO_2 adsorption/desorption behavior.

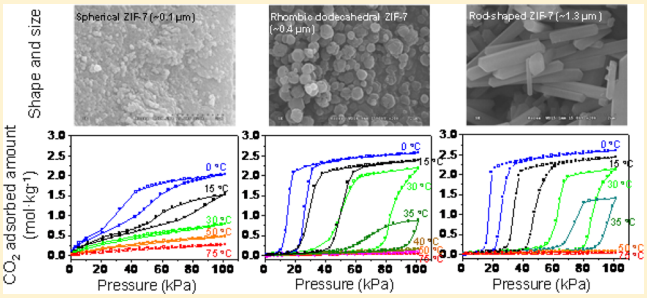

1. INTRODUCTION

Among metal−organic frameworks, zeolitic imidazolate frameworks (ZIFs) have attracted the attention of researchers as an alternative to other microporous materials including zeolites because of their promising properties such as large surface area, facile synthesis, and controllable pore size.[1−3] In particular, ZIFs are known for their high chemical and thermal stabilities, which are primarily due to the strong bonding among their components.[4] Indeed, the use of ZIFs has been reported in many applications, including sensors,[5,6] catalysts,[7] catalyst supports,[8] selective layers on catalysts via encapsulation,[9−11] adsorbents,[12,13] matrix fillers,[14−17] membranes,[13,18−22] drug delivery,[23,24] and so on.

In particular, on the basis of molecular dynamics simulations,[25,26] ZIF-7 is expected to exhibit high hydrogen permselectivity, making it a good candidate for establishing a continuous hydrogen-selective membrane. Indeed, ZIF-7 membranes have been experimentally demonstrated as effective for H_2/CO_2 separations in precombustion processes.[13,27] However, the thermal stability of ZIF-7, which presumably affects its intrinsic properties (including adsorption capacities) in the long term, has not yet been rigorously investigated, despite its importance for practical and reliable applications.

Received: February 16, 2014
Published: May 9, 2014

dx.doi.org/10.1021/ja5016298 | J. Am. Chem. Soc. 2014, 136, 7961−7971

To the best of our knowledge, Park et al.[4] first reported the chemical and thermal stabilities of ZIF-7 along with other types of ZIFs. Chemical stability tests have been conducted via monitoring of X-ray diffraction (XRD) patterns of ZIF-7 immersed in various solvents (e.g., benzene, water, ethanol, etc.) at different temperatures and duration times, while the thermal stability has been examined via thermogravimetric analysis (TGA). Recently, a study related to structural changes in ZIF-7 due to thermal treatment was reported; interestingly, structural changes due to the removal of occluded water inside the as-synthesized ZIF-7 resulted in restoration of the original ZIF-7 phase after CO_2 readsorption.[28] This indicated the successful incorporation of CO_2 within the ZIF-7 framework, accompanying recovery of the original ZIF-7 phase. More recently, ZIF-7 phase reversibility was also evidenced via readsorption of ethanol or *N*,*N*-dimethylformamide (DMF),[29] indicating the importance of the adsorption−desorption of guest molecules in determining the structure and, accordingly, the interactions between the guest molecules and the host ZIF-7 framework.

In most practical applications (adsorptions, membranes, catalyst supports or selective layers, etc.), the activation of as-synthesized ZIF-7s via the elimination of occluded water and/or solvent is necessary to fully open the pore space. Despite previous demonstrations of interesting reversible phase transition features due to the presence of certain guest molecules,[28,29] the structural changes of ZIF-7 should be appropriately correlated with its properties according to desired applications. Especially, the properties of ZIF-7 in which organic compounds are incorporated into the framework should not be regarded as similar to the properties of conventional inorganic materials such as zeolites.[30] For example, ZIF-7 activation via thermal treatment has been shown to induce a structural change in ZIF-7.[28,29] Accordingly, the phase transition should be crystallographically deciphered and its effect on properties should be studied. On this basis, the experimental properties of activated ZIF-7s can be correlated with their structural information; furthermore, the appropriate simulations and/or theoretical studies can be beneficial in predicting their properties as necessary.[31,32] In addition, an accurate understanding of the characteristics of ZIF-7s is critical for their use in desired applications. For example, an appropriate activation process is required in order to avoid the defect formation in ZIF-7 membranes that results from a difficult removal of guest molecules.[21] Under this circumstance, an effective strategy should be developed, as exemplified by solvent exchange prior to activation for less-defective ZIF-78 membrane formation.[33]

N_2 physisorption analysis, although widely used to analyze pore structures in microporous materials, has shown significant inconsistencies in several ZIF-7 materials.[14,34,35] This uncommon result might indicate that the pore structure of ZIF-7 is a considerably sensitive function of its synthetic origin and/or post-treatment method and is thus potentially different in the final pore mouth and/or channel topology, resulting in a surface resistance or barrier.[36−39] In addition, CO_2 adsorption isotherms in ZIF-7 at temperatures greater than 0 °C are in good agreement among the data reported in the literature,[28,29,40] showing (1) similar CO_2 saturation capacities and (2) the presence of hysteretic adsorption/desorption behaviors. Nevertheless, to the best of our knowledge, the effects of the shape and size of ZIF-7 on its CO_2 adsorption properties has not been intensively studied to date despite its importance in practical applications such as adsorption- and membrane-based methods for effective CO_2 separations in both pre- and postcombustion processes.[13,41]

To this end, a rigorous investigation of the thermal stability of ZIF-7 and its CO_2 adsorption properties is highly desirable as a starting point, and to the best our knowledge, the present study is the first attempt for this purpose. Here we employed three ZIF-7s possessing different shapes and sizes. Although TGA results suggested the higher thermal stability of ZIF-7s under air even at ∼400−550 °C,[4,15,17,20] XRD indicated that the ZIF-7 structure had already been converted into zinc oxides at ∼400 °C, requiring careful consideration under oxidative conditions. Surprisingly, the guest molecules inside the three ZIF-7s consisted mainly of DMF, not water as reported in the literature.[4] As inconsistent data for identifying guest molecules inside ZIF-7s have been reported,[17,20,42] the use of complementary characterization tools (here, C/H/N elemental analysis, TGA, and FT-IR spectroscopy) is highly desirable to obtain accurate information.

Finally, we measured the CO_2 adsorption isotherms of the three activated ZIF-7s. Despite their identical ZIF-7 crystal structures, they showed distinctive CO_2 adsorption isotherms, indicating a difference in their pore structures at the molecular level. Almost reversible CO_2 adsorption/desorption isotherms were for the first time observed for the smallest ZIF-7 (∼100 nm) and are seemingly due to the flexible pore structure near and on its outer surface. On the contrary, as previously reported,[28,29,40,44] hysteretic CO_2 adsorption/desorption behaviors were detected for the other larger ZIF-7s, plausibly as a result of their nonpreferred interaction with CO_2. On the basis of the fundamental understanding of these unique CO_2 adsorption properties, the deliberate choice and effective control of the ZIF-7 pore structure are necessary for its realization in energy-efficient CO_2 capture.

2. EXPERIMENTAL SECTION

2.1. Synthesis of ZIF-7 Particles. First, spherical ZIF-7 was synthesized using a reported method.[20] Specifically, 0.77 g of benzimidazole (bim) (98%, Sigma-Aldrich) and 0.3 g of zinc nitrate hexahydrate, $Zn(NO_3)_2{\cdot}6H_2O$ (98%, Sigma-Aldrich), were added to ∼100 mL of DMF (99%, Sigma-Aldrich) in a 500 mL plastic bottle. For convenience, bIM is used to represent benzimidazolate in the ZIF-7 structures. The final molar composition of the synthesis solution was 0.15 Zn^{2+}:1 bim:200 DMF. After reaction at room temperature for 2 days under stirring, the solid product was centrifuged and washed with DMF three times. The recovered product was further dried at room temperature. For convenience, this sample is denoted as ZIF-7-S, where S represents the spherical morphology of ZIF-7.

Second, rod-shaped ZIF-7 was synthesized using a reported method.[43] Briefly, 0.31 g of bim and 0.27 g of zinc chloride, $ZnCl_2$ (99%, Sigma-Aldrich), were added to ∼30 mL of DMF contained in a Teflon liner, followed by the addition of 0.47 g of diethylamine (DEA) (99.5%, Sigma-Aldrich). The final molar composition of the synthesis solution was 0.74 Zn^{2+}:1 bim:150 DMF:2.4 DEA. The Teflon liner containing the reaction solution was sealed in an autoclave and rotated at ∼40 rpm for 24 h in an oven preheated to 130 °C. After completion of the reaction, the autoclave was quenched in tap water. The product was centrifuged, washed with DMF three times, and further dried at room temperature. This sample is denoted as ZIF-7-R, where R represents the rod morphology of ZIF-7.

Finally, rhombic-dodecahedral ZIF-7 particles were synthesized using a procedure developed in this study. For the synthesis, 0.41 g of bim and 0.56 g of zinc acetate dihydrate, $Zn(CH_3COO)_2{\cdot}2H_2O$ (99%, Sigma-Aldrich), were added to ∼30 mL of DMF in a Teflon liner, followed by the addition of 3.14 g of DEA. The final molar composition of the synthesis solution was 0.75 Zn^{2+}:1 bim:110

dx.doi.org/10.1021/ja5016298 | J. Am. Chem. Soc. 2014, 136, 7961−7971

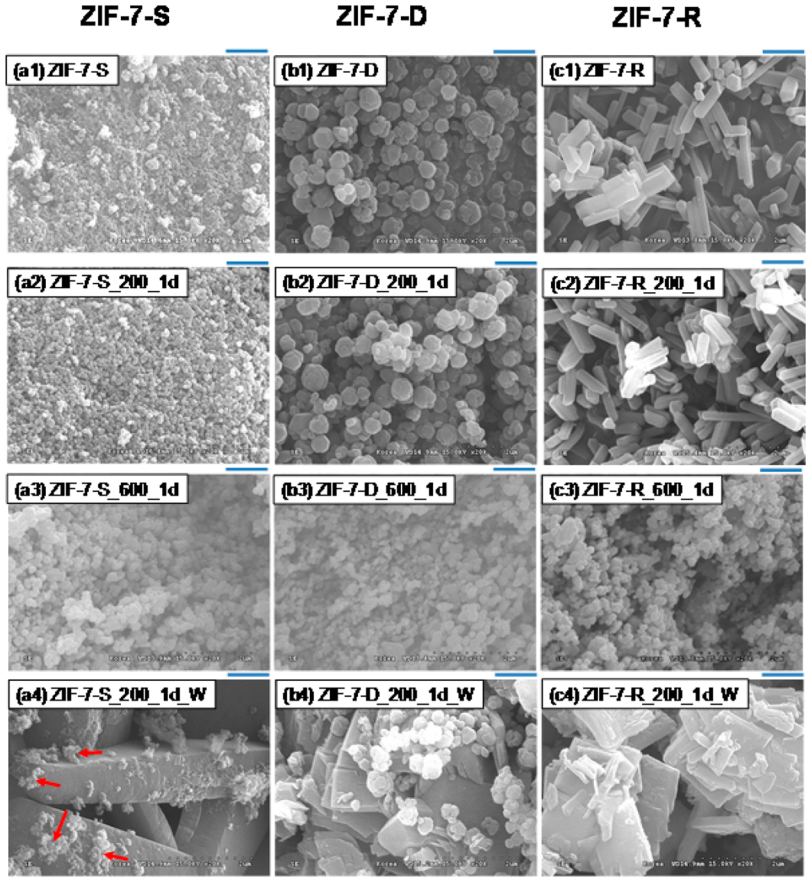

Figure 1. (a1−c3) SEM images of (a1) ZIF-7-S, (b1) ZIF-7-D, and (c1) ZIF-7-R (first row) and particles obtained after heat treatments of ZIF-7-x (x = S, D, R) at (a2−c2) 200 °C (second row) and (a3−c3) 600 °C (third row). For the heat treatment, dried samples were exposed to 200, 300, 400, 500, and 600 °C for 1 day under air; these are denoted as ZIF-7-x_*y*_1d (x = S, D, R; *y* = 200, 300, 400, 500, 600). For clarity, the SEM images of ZIF-7-x_*y*_1d (*y* = 200 and 600) are shown here, while the complete set of SEM images is displayed in Figure S1 in the Supporting Information. (a4−c4) SEM images of particles ZIF-7-x_200_1d_W (x = S, D, R, respectively) recovered after immersion of ZIF-7-x_200_1d in water for 7 days (last row). Scale bars above the SEM images indicate 1 μm.

DMF:12.5 DEA. The Teflon liner containing the reaction solution was sealed in an autoclave and rotated at ∼40 rpm for 48 h in an oven preheated to 130 °C. After completion of the reaction, the autoclave was quenched in tap water. The product was centrifgued, washed with DMF three times, and further dried at room temperature. This sample is denoted as ZIF-7-D, where D represents the dodecahedron in the rhombic-dodecahedral morphology of ZIF-7, similar to a previous study.[44] The yields of ZIF-7-S, -D, and -R were estimated as ∼60, ∼70, and ∼20%, respectively.

In addition to the three synthetic approaches for ZIF-7, another synthesis in ethanol or methanol media was performed in an attempt to ascertain the effect of the solvent on the ZIF-7 synthesis. About 0.77 g of bim and 0.3 g of $Zn(NO_3)_2{\cdot}6H_2O$ were added to ∼100 mL of ethanol (99.5%, Sigma-Aldrich) or methanol (99.85%, Sigma-Aldrich) in a 500 mL plastic bottle, giving a final molar composition of 0.15 Zn^{2+}:1 bim:260 ethanol or 380 methanol. After completion of the reaction at 30 °C for 2 days under stirring, the solid product was centrifuged and washed with the respective solvent (ethanol or methanol) three times. The recovered product was further dried under ambient conditions. For convenience, the samples obtained as described above are denoted as E_30 and M_30, where E and M represent ethanol and methanol solvents, respectively, and 30 indicates the reaction temperature (in °C).

Synthesis using ethanol as the solvent was also attempted at a higher temperature of 130 °C with a different additive. First, 0.31 g of bim and 0.58 g of $Zn(NO_3)_2{\cdot}6H_2O$ were added to ∼30 mL of ethanol in a Teflon liner, with the subsequent addition of 0.47 g of DEA. Second, 0.31 g of bim and 0.27 g of $ZnCl_2$ were added to ∼30 mL of ethanol in a Teflon liner, with subsequent addition of 0.35 g of sodium formate, NaCOOH (99%, Sigma-Aldrich), to the mixture. The final molar compositions of the two synthesis solutions were: (1) 0.74 Zn^{2+}:1 bim:200 ethanol:2.4 DEA and (2) 0.74 Zn^{2+}:1 bim:200 ethanol:2 NaCOOH, respectively. The Teflon liners containing the reaction solutions were sealed in autoclaves and rotated at ∼40 rpm for 2 days in an oven preheated to 130 °C. After completion of the reaction, the autoclave was quenched in tap water. The product was recovered as was done for E_30. For convenience, the resulting particles based on the above two synthetic approaches are denoted as E_130_1 and E_130_2, respectively, where 130 indicates the synthesis temperature (in °C).

2.2. Stability Tests of ZIF-7 Particles. The three ZIF-7-x (x = S, D, R) materials were heat-treated at temperatures of 110, 200, 300, 400, 500, and 600 °C for certain times using a furnace (CRF-M20-UP, Plusko-lab, South Korea) or an oven (DX302, Yamato Scientific Co., Japan) under air. For convenience, a ZIF-7-x sample heat-treated at *y* °C for a duration of z (e.g., z = 1d for a duration of 1 day) is denoted as ZIF-7-x_*y*_z. Some ZIF-7-x (x = S, D, R) samples were heat-treated in a vacuum oven (OV-11, JEIO TECH, South Korea) at 200 °C; these are denoted as ZIF-7-x_*y*_z_V, where V indicates the vacuum condition. In addition, ZIF-7 particles that had already been heat-treated (ZIF-7-x_200_1d; x = S, D, R) were tested following two approaches to determine ZIF-7 structure reversibility via water adsorption; they were exposed to ambient conditions for ∼2 days and were also immersed in deionized (DI) water and agitated using a shaker (SI-300R, Lab Companion) for ∼7 days. The resulting sample after immersion in DI water is denoted as ZIF-7-x_200_1d_W, where W indicates immersion in water.

dx.doi.org/10.1021/ja5016298 | *J. Am. Chem. Soc.* 2014, 136, 7961−7971

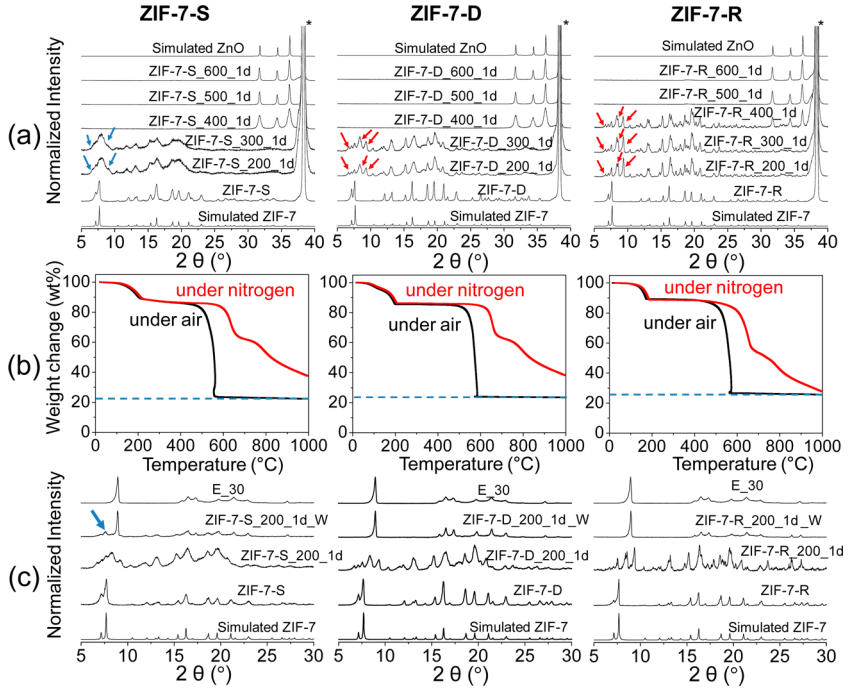

Figure 2. (a) XRD patterns of ZIF-7-S (left), -D (middle), and -R (right) along with those obtained after heat treatments. For the heat treatment, dried samples were exposed to 200, 300, 400, 500, and 600 °C for 1 day under air; ZIF-7-x_*y*_1d (x = S, D, R; *y* = 200, 300, 400, 500, 600). The simulated XRD patterns of zinc oxide and ZIF-7 are included for comparison, and asterisks in the XRD patterns indicate the peaks from the aluminum sample holder. (b) TGA results for ZIF-7-S (left), -D (middle), and -R (right) in air (black) and nitrogen (red) environments. (c) XRD patterns of ZIF-7-x, ZIF-7-x heat-treated at 200 °C for 1 day under air, and ZIF-7-x immersed in water under ambient conditions for 7 days [x = S (left), D (middle), R (right)]. For comparison, the XRD pattern of E_30, a phase obtained in ethanol solvent instead of DMF, has also been included at the top.

2.3. Characterizations. Scanning electron microscopy (SEM) images of ZIF-7 crystals were acquired using a field-emission scanning electron microscope (Hitachi S-4300). A Pt layer was coated onto each sample via ion sputtering (Hitachi E-1030). XRD patterns of ZIF-7 before and after heat treatments under air were acquired in the $\theta/2\theta$ configuration using a Rigaku D/Max-2500 V/PC diffractometer (Japan) with Cu Kα radiation (40 kV, 100 mA, λ = 0.154 nm). For comparison, a simulated XRD pattern of ZIF-7 was generated using Mercury software [available from the Cambridge Crystallographic Data Centre (CCDC), www.ccdc.cam.ac.uk]. For simulation, a crystallographic information file (CIF) for ZIF-7 was obtained from the CCDC Web site (deposition number 602541).[4] In addition, temperature-programmed XRD measurements were performed using an Empyrean diffractometer (PANalytical) with monochromatized Cu Kα radiation (λ = 1.54056 Å). The diffractometer was equipped with an in situ chamber (HTK-16N, Anton Paar) and a temperature control unit (TCU 200N, Anton Paar). A sample was dispersed in ethanol and then deposited on a Pt strip. While the temperature was increased from 25 to 700 °C, in situ XRD patterns were collected isothermally at intervals of 100 °C. During the measurement, the chamber was filled with an atmosphere of argon (for inert conditions) or air (for oxidative conditions). N_2 physisorption isotherms at 77 K and CO_2 adsorption isotherms at different temperatures (0–75 °C) of ZIF-7s were measured using an ASAP 2020 instrument (Micromeritics, Inc.). In order to eliminate undesired sorption during storage, both thermally activated ZIF-7-x_200_2d and ZIF-7-x_200_1d_V (x = S, D, R) particles were further degassed at ~120 °C overnight before measurements. In addition, unknown phases (i.e., E_130_1 and E_130_2) were used to acquire the N_2 physisorption isotherm at 77 K and the CO_2 adsorption isotherm at 30 °C; these samples were also degassed at ~120 °C at least overnight before measurements. For TGA measurements, ZIF-7 particles dried at room temperature were heated to ~1000 °C at a ramp rate of ~5 °C·min^{-1} under either air or N_2 (SDT-Q600, TA Instruments).

3. RESULTS AND DISCUSSION

Figure 1a1–c1 illustrates the differing shapes and sizes among the three ZIF-7 types: spherical, rhombic-dodecahedral, and rod-shaped morphologies were observed for ZIF-7-S, -D, and -R, respectively, with corresponding sizes of ~100, ~400, and ~1300 nm in the longest dimension. The common feature shared by these three materials is the ZIF-7 structure; however, their differing geometries and sizes make them good standard materials for comparing the thermal stabilities of ZIF-7 while considering kinetic effects.

Figure 2a shows the XRD patterns of ZIF-7-S, -D, and -R particles and the corresponding XRD patterns after heat treatment at 200–600 °C for 1 day under air (i.e., ZIF-7-x_*y*_1d; x = S, D, R; *y* = 200, 300, 400, 500, 600). After heat treatments at 200 and 300 °C, the sharp peaks of ZIF-7-S broadened in general. This possibly indicates a reduction in its effective particle size due to some detachment of the initially aggregated as-synthesized ZIF-7 particles during heat treatment, though it was not pronounced in the SEM images (Figure 1a1,a2). After heat treatments at higher temperatures (above 400 °C), the initial ZIF-7-S was totally converted into zinc oxide, as confirmed by the simulated XRD pattern of zinc oxide. This result can be interpreted to occur because zinc atoms incorporated in the ZIF-7 framework apparently become dissociated and fully oxidized by oxygen in air at high temperatures. In addition to this obvious outcome, it was noted that additional peaks appeared for ZIF-7-S after heat treatments at 200 and 300 °C, as indicated by the blue arrows in Figure 2a. For convenience, this phase is denoted as ZIF-7-S-I, where I refers to an intermediate phase en route to the final zinc oxide phase.

dx.doi.org/10.1021/ja5016298 | J. Am. Chem. Soc. 2014, 136, 7961–7971

The observation of such additional peaks was reported in recent studies.[28,29] In particular, those additional peaks disappeared specifically above a certain pressure of CO_2 (~60 kPa) at 30 °C, resulting in recovery of the original ZIF-7-S XRD pattern after CO_2 readsorption. This reversibility of the XRD pattern of ZIF-7 was attributed to the replacement of the positions inside ZIF-7 originally occupied by water with CO_2. Similar changes in the XRD patterns due to heat treatments were observed for ZIF-7-D and -R, although the additional peaks appearing after 200 °C (indicated by the red arrows for ZIF-7-D and -R in Figure 2a) were sharper that those for ZIF-7-S. In this form, ZIF-7-D and -R can also be denoted as ZIF-7-D-I and -R-I, respectively, based on the naming of ZIF-7-S-I; furthermore, these materials are denoted as ZIF-7-I for the general expression of the intermediate phase regardless of type. In view of the fact that the ZIF-7 phase transition into the zinc oxide form is a kinetically limited process given the duration time (here, 1 day), the coexisting XRD patterns of ZIF-7-R-I and zinc oxide for ZIF-7-R_400_1d (Figure 2a) suggested that the structural transition was a function of ZIF-7 size, apparently reflected by the longer characteristic length of ZIF-7-R compared with ZIF-7-S and -D (Figure 1a1−c1). In other words, the temperature delay for the transformation of ZIF-7-R toward ZnO can be ascribed mainly to the mass transport limitation during oxidation because of its much larger dimensions compared with those of ZIF-7-S and -D.

As shown in Figure 1a1−a3 and Figure S1 in the Supporting Information, we could not distinguish any difference in ZIF-7-S shapes or sizes before and after heat treatments up to 600 °C under the SEM resolution, although XRD patterns (Figure 2a) confirmed that ZIF-7-S exposed to temperatures greater than 400 °C was already converted into the zinc oxide phase. In contrast, the shape of ZIF-7-D was well-preserved under heat treatment for up to 1 day at 300 °C, with a dramatic change to the globular shape above 400 °C (Figure 1b1−b3 and Figure S1), where a phase transition to zinc oxide was confirmed by the XRD pattern (Figure 2a). In addition, the rod shape of ZIF-7-R was preserved up to a heat treatment temperature of 400 °C (Figure 1c1−c3 and Figure S1), seemingly as a result of its longer dimension compared with ZIF-7-S and -D, as also supported by the XRD patterns in Figure 2a. As expected, although a minor zinc oxide phase was observed in ZIF-7-R at 400 °C, the eventual complete change to the zinc oxide phase was also observed beyond 500 °C, yielding a final globular shape similar to that for the other two materials.

TGA characterization is often adopted to show the thermal stability of ZIF-7 materials.[4,20] On the basis of TGA, ZIF-7 was previously established as having thermal stability in either N_2 or air environments up to ~400−500 °C.[4,15,17,20] TGA results for all three ZIF-7 types (Figure 2b) also indicate that the weight changed, mainly because of the desorption of guest molecules at ~200 °C, with no distinct change observed up to ~400−450 °C. With respect to the empirical formula of $Zn(bIM)_2{\cdot}(H_2O)_3$ for ZIF-7,[4] its initial weight change as a result of water removal was estimated as ~15.3%, which was close to the measured value of 12.8% for ZIF-7-S. However, its C/H/N elemental composition (C, 54.0 ± 1.3; H, 4.2 ± 0.5; N, 19.3 ± 0.6; see Table S1 in the Supporting Information) was different from the counterpart according to the above empirical formula (C, 47.54; H, 4.56; N, 15.84).[4] Considering the both presence of H_2O and DMF in the as-synthesized ZIF-7-S, the empirical formula for ZIF-7-S was estimated to be $Zn(bIM)_2{\cdot}(DMF)_{0.5\pm0.1}{\cdot}(H_2O)_{0.5\pm0.5}$. It appears that the water content had a higher uncertainty than the DMF content. The presence of DMF was also supported by the FT-IR results for the as-synthesized ZIF-7-S (Figure S2), while the amount of H_2O was significantly negligible, validating the aforementioned uncertainty in the H_2O fraction. At this point, it would be reasonable to assume that a majority of the guest molecules were DMF solvent molecules, though we cannot completely rule out the presence of some H_2O. This leads to the empirical formula $Zn(bIM)_2{\cdot}(DMF)_{0.6}$, which is then close to the one reported in a previous study by Kang et al.[15] The estimations based on both elemental analysis and TGA results for ZIF-7-D and -R resulted in the comparable empirical formulas $Zn(bIM)_2{\cdot}(DMF)_{0.68}$ and $Zn(bIM)_2{\cdot}(DMF)_{0.52}$, respectively. In Figure 2b, the presence of zinc oxide due to the complete oxidation of zinc atoms in ZIF-7s under air accounted for ~22.3, ~23.5, and ~25.6 wt % portions for ZIF-7-S, -D, and -R, respectively (Table S1). Those measured values for ZIF-7-x (x = S, D, R) were in good agreement with the values of ~23.7, ~23.3, and ~24.1% calculated from the respective empirical formulas. Although the conclusion that ZIF-7 is stable up to ~400−450 °C in either air or N_2 environments, similar to the results of previous studies,[4,15,17,20] can be drawn from the TGA results shown in Figure 2b, the XRD patterns in Figure 2a verified a structural change of ZIF-7 eventually toward the zinc oxide phase due to the heat treatment under air.

We found that there have been inconsistent results in the literature for deriving the empirical formula. For example, the TGA result around 300 °C showed ~15.8 wt % loss,[20] which was similar to the original experimental value of 15.8 wt %.[4] However, the fraction of zinc oxide under oxidative conditions was 32.7 wt %, which was significantly different from the theoretical value of 23.0 wt %. On the other hand, it was reported that the molecule inside ZIF-7 was DMF, not H_2O, though the corresponding FT-IR spectra exhibited the presence of H_2O.[15] In addition, the C/H/N elemental analysis results in a recent work[42] were close to those reported by Park et al.,[4] indicating that the empirical formula was also $Zn{\cdot}(bIM)_2{\cdot}(H_2O)_3$. However, the corresponding weight loss up to 300 °C (~6.1%) was much smaller than the expected value (15.8%), and the FT-IR results also indicated the presence of DMF in the as-synthesized ZIF-7 to some extent. These inconsistent reports support the importance of the rigorous, accurate characterization of ZIF-7s as demonstrated in this study and the need to use multiple characterization methods for reasonable validation. At this point, we would like to emphasize that on the basis of the accurate understanding of ZIF-7, the thermal activation processes required for full opening of the pore space should be appropriately conducted for desired applications, as exemplified by a novel strategy to lead to less-defective ZIF membranes via the effective removal of guest molecules (e.g., DMF).[21,33]

We further investigated the structural change of ZIF-7 by varying the heat treatment time up to 7 days at 200 °C. Figure S3 shows the XRD patterns of ZIF-7-x_200_z (x = S, D, R; z = 12 h, 1 day, 2 days, and 7 days). In all three samples, ~12 h exposure at 200 °C led to similar changes in the XRD patterns, and the resulting XRD patterns were maintained for up to ~7 days without further noticeable changes; this implies that the structural change was primarily due to the removal of guest molecules (mainly, DMF), as indicated by TGA in Figure 2b. However, no apparent difference in ZIF-7 shapes was noted before and after heat treatment at 200 °C (Figure 1a1−c1 and Figure S4).

dx.doi.org/10.1021/ja5016298 | J. Am. Chem. Soc. 2014, 136, 7961−7971

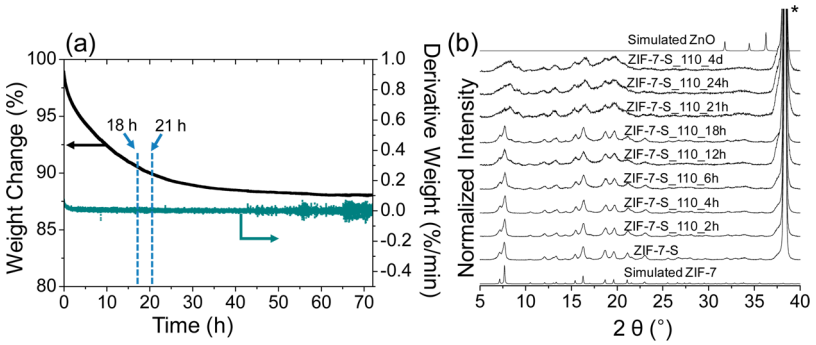

Figure 3. (a) TGA results for ZIF-7-S at 110 °C as a function of time. (b) XRD patterns of ZIF-7-S after the exposure to 110 °C under air over varying durations (2 h to 4 days), along with the simulated XRD patterns of zinc oxide and ZIF-7.

Figure S5 shows the XRD patterns of ZIF-7-S after heat treatments at 400 °C with varying duration times (up to 24 h). Even after a short time of 2 h, the above-mentioned typical change in the XRD patterns (Figure 2a) was also clearly evident, indicating the facile removal of guest molecules at the higher temperature (400 °C). Unlike the heat treatment at 200 °C, additional peaks between ∼31 and 36° appeared after treatment for ∼12 h and became gradually more pronounced with increased time. A treatment time of 20 h was sufficient for conversion of the ZIF-7 phase to the zinc oxide phase. This kinetic study of the structural change of ZIF-7-S at 400 °C indicated that as guest molecules were totally desorbed from the ZIF-7-S framework, broadened XRD peaks were initially observed along with the appearance of the additional peaks (corresponding to ZIF-7-S-I); as time further elapsed, the ZIF-7-S-I phase began to collapse and rearrange, resulting in the total conversion to the zinc oxide phase. Along with the XRD patterns in Figure 2a, this supports the conclusion that the zinc in the original ZIF-7 was gradually oxidized with increasing time under air and eventually converted into zinc oxide.

As previously reported,[28] one may expect that the removal of water and/or solvent in ZIF-7 induces its structural change. In order to confirm this, we traced the transient weight change of ZIF-7-S mainly due to the gradual removal of guest molecules (i.e., DMF along with very little H_2O) at ∼110 °C (Figure 3a) and analyzed the corresponding XRD patterns in order to correlate the structural change with the amount of guest molecules inside ZIF-7-S (Figure 3b). Figure 3a shows that as guest molecules were quickly removed from ZIF-7-S up to ∼10 h and then were slowly desorbed, a plateau was reached after ∼24 h. The ZIF-7-S phase appeared to be well-preserved up to ∼18 h. However, after ∼21 h, especially when the guest molecules were almost removed (Figure 3a), the ZIF-7 phase was then transformed into the aforementioned intermediate phase (i.e., ZIF-7-S-I). On the basis of both the TGA and XRD characterizations, one may conclude that the structural change in ZIF-7-S can be strongly ascribed to the complete elimination of guest molecules in ZIF-7-S. Recently, the ZIF-7 phase accompanied by an additional phase was reported for a ZIF-7 sample after heat treatment at 200 °C prior to CO_2 adsorption isotherm measurements.[28] On the basis of the current study, the XRD pattern in that study indicated that the occluded water was successfully removed by degassing processes. However, in a more recent study,[35] although as-synthesized ZIF-7 was dried at 130 °C before characterizations, the corresponding XRD pattern was still similar to that of as-synthesized ZIF-7. As a possible reason, solvent exchange of the as-synthesized ZIF-7 with methanol allowed its substitution for water, and the subsequent elimination of methanol did not induce the phase change; otherwise, the water or methanol was not fully removed during drying, though pretreatments in that study (∼155 °C for 3 h under vacuum) for measuring N_2 physisorption and CO_2 adsorption isotherms were likely sufficient for removal purposes. At that time, the XRD pattern would be similar to that of the ZIF-7-I phase. This demonstrates the importance of deliberate handling of ZIF-7 for its appropriate use due to its intrinsic properties, especially via the accurate understanding of post-treatments and the corresponding structural information.

Despite an indirect investigation, we exposed ZIF-7-x_200_1d (x = S, D, R) to ambient conditions in order to determine whether it could possibly be converted back into the original ZIF-7 via adsorption of water vapor in the air. However, exposure of ZIF-7-x_200_1d (x = S, D, R) to ambient conditions for up to ∼2 days did not result in a reversible transition to the original ZIF-7-S, suggesting an insufficient amount of adsorbed water vapor to regenerate the original ZIF-7 (Figure S6). This can be attributed to the low rate of diffusion of water into the ZIF-7-I phase and the low water vapor pressure (∼3 kPa) as a driving force at room temperature. Instead, we immersed ZIF-7-x_200_1d samples (x = S, D, R) in DI water and left them for 7 days to expedite water adsorption; Figure 2c shows that the immersion of the three ZIF-7s in water rather caused the phase transition to an unknown phase, which was coincidentally similar to that obtained after synthesis in ethanol or methanol media instead of DMF (Figures S7 and S8). Unlike ZIF-7, the unknown phase was well-preserved after heat treatment at 200 °C for 1 day (Figure S8). For convenience, the unknown phase is denoted as phase X from now on. Such a phase has recently been reported in the literature for an attempted ZIF-7 synthesis in a water/ethanol mixture.[29] Compared with the synthesis at room temperature, the XRD patterns of phase X were more pronounced for the synthesis at a higher temperature of 130 °C (Figure S9). Despite the improved crystallinity at that temperature, N_2 physisorption and CO_2 adsorption isotherms (Figure S9) suggest that the unknown phase X was considerably dense with no accessible microporous structures and was of no use for any practical membrane- or adsorption-based separations.

Figure 1a4−c4 and Figure 2c reveal that the exposure of ZIF7_S_200_1d to liquid water resulted in not only the phase transition to phase X but also its concomitant morphological change. After its immersion in water, the small globular ZIF-7-S was changed to particles consisting mainly of large parallelopipedons. Some residual globular ZIF-7-S particles

dx.doi.org/10.1021/ja5016298 | J. Am. Chem. Soc. 2014, 136, 7961−7971

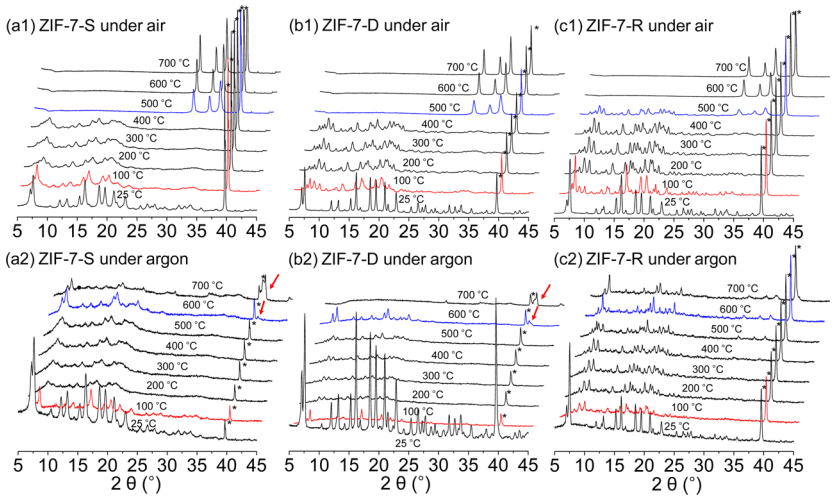

Figure 4. Temperature-programmed XRD patterns measured under (a1−c1) air and (a2−c2) argon flows for ZIF-7-S, -D, and -R, respectively. Asterisks denote the XRD peaks attributed to the Pt sample holder. For clear comparison, the XRD patterns at 100 °C are marked in red and the XRD patterns that indicate phase conversion to zinc oxide under air (upper row) or thermal degradation under argon (lower row) are marked in blue.

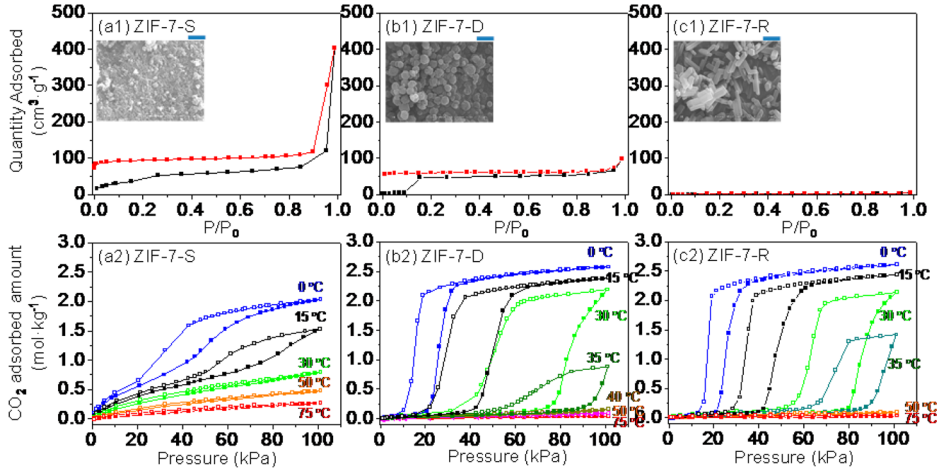

Figure 5. (a1−c1) N_2 physisorption (upper row) and (a2−c2) CO_2 adsorption isotherms (lower row) of ZIF-7-S_200_2d (left), -D_200_2d (middle), and -R_200_2d (right) particles. For N_2 physisorption, black and red points represent adsorption and desorption, respectively, while for CO_2 adsorption, solid and open points indicate adsorption and desorption, respectively. The SEM images of ZIF-7-x (x = S, D, R) from Figure 1a1−c1, respectively, are shown in the insets of (a1−c1) for size comparison.

(indicated by red arrows in Figure 1a4), apparently in the process of transformation to the final unknown phase X, were also observed on the outer surface of the parallelopipedons. The existence of residual ZIF-7-S was noted by the retention of the main XRD pattern of ZIF-7-S (indicated by a blue arrow in Figure 2c). A similar morphological change after water immersion for 7 days was also observed for the other ZIFs, as shown in panels b4 and c4 of Figure 1. At this point, it is worth mentioning that despite differences in the synthetic routes for the ZIF-7s and E_30 or M_30, the immersion of ZIF-7s in water resulted in an identical crystal structure but a different crystal shape (Figure 1a4−c4 and Figure S7).

Unlike the manifest feature whereby full oxidation of zinc atoms in ZIF-7 results in a zinc oxide phase (Figure 2a), we conjectured that an inert environment would not lead to the ZIF-7 phase change until a certain temperature, where thermal degradation and concomitant structural collapse take place. In order to confirm this, we acquired temperature-programmed XRD patterns of all three ZIF-7s under both air and argon flows (Figure 4). Under air, XRD patterns similar to those observed in Figure 2a were also recognized; new XRD peaks in addition to those of ZIF-7 (corresponding to the ZIF-7-I phase) appeared at ∼200 °C, and the ZIF-7-I phase was further converted into zinc oxide at a temperature higher than ∼400 °C. Among the three, the XRD patterns at ∼500 °C for ZIF-7-R revealed the coexistence of ZIF-7-R-I with zinc oxide, as opposed to the ZIF-7-S and -D, which were completely transformed to zinc oxide at that temperature. On the contrary, under inert argon flows, all three ZIF-7 structures were well-preserved, even at 500 °C, in the form of the ZIF-7-I phase. As the heat treatment temperature was increased to 600 °C, the XRD patterns corresponding to the ZIF-7-I phase were transformed either to a new unidentified phase (for ZIF-7-S and -D) or coexisted with the unidentified phase (for ZIF-7-R). The new peaks around $2\theta = 40°$ (indicated by red arrows in Figure 4a2,b2) accompanied the appearance of the unidentified phase for ZIF-7-S and -D. Heat treatment at a higher temperature (≥700 °C) under argon flows is likely to

dx.doi.org/10.1021/ja5016298 | J. Am. Chem. Soc. 2014, 136, 7961−7971

completely collapse the unidentified phase, as shown for ZIF-7-D (Figure 4b2). As the largest ZIF-7-R showed the highest structural stability under air conditions (Figure 2a and Figure 4a1−c1), the XRD pattern corresponding to the unidentified phase in the largest ZIF-7-R were also preserved at a higher temperature (here, 700 °C) under an argon flow. Interestingly, the XRD patterns stemming from the smallest ZIF-7-S showed the existence of the unidentified phase at 700 °C under an argon flow, while the XRD pattern almost disappeared at the same temperature for the larger ZIF-7-D counterpart under an argon flow. This possibly suggests that thermal degradation was retarded in the aggregated form of ZIF-7-S, though the ZIF-7-S particles were smaller than the ZIF-7-D particles.

Temperature-programmed XRD analysis (Figure 4) indicates that the structural integrity of ZIF-7 was strongly correlated to the thermal treatment employed (i.e., temperature and environment). Indeed, ZIF-7, which is known for its high thermal stability,[1,4] displayed thermal stability up to ∼500 °C under inert conditions, though longer exposure tests are necessary to confirm this. This result is a reflection of the strong interaction between the benzimidazolate ligands and zinc atoms; however, when activation processes that are mainly targeted to remove water and/or solvent must be conducted under air or any oxidative conditions, careful attention should be paid to avoid the undesired phase transition. The activation process at ∼200 °C under air, as supported by the long-term heat treatment up to 7 days (Figure S3), appears to be desirable for ZIF-7, especially in eliminating DMF and/or water and thus fully opening the interior pores. FT-IR spectra of the ZIF-7-I phase (Figure S2) also evidenced the successful removal of the guest molecules after heat treatments at 200 °C.

Recognizing discrepancies in the N_2 physisorption results in the literature,[14,34] we also measured N_2 physisorption isotherms at 77 K for all three ZIF-7 samples (Figure 5a1−c1). In particular, heat-treated ZIF-7 samples (i.e., ZIF-7-x_200_2d), which apparently contained no guest molecules, were chosen for adsorption measurements in an attempt to ascertain their representative features. Figure 5a1−c1 demonstrates that the N_2 physisorption results for the three samples were considerably different as well, and the corresponding external surface areas extracted from Brunauer−Emmett−Teller (BET) analysis (∼150, ∼25, and ∼4 $m^2 \cdot g^{-1}$ for ZIF-7-S, -D, and -R, respectively; Table S2) indicated that N_2 was mainly physisorbed on the external surface and thus that N_2 physisorption was dependent on their particle sizes. In addition, CO_2 adsorption isotherms for all three ZIF-7s were measured in the range of 0−75 °C (Figure 5a2−c2). The CO_2 adsorption isotherms of ZIF-7-D and -R were similar to those reported in previous studies[28,29,40,45] with respect to CO_2 saturation capacity (∼2−3 $mol \cdot kg^{-1}$) and the presence of hysteresis. However, the CO_2 adsorption isotherms of ZIF-7-S were totally distinct, especially at 30−75 °C, the typical temperatures of flues gases generated from a coal-fired power plant:[41] they exhibited both identical adsorption and desorption points and a reduced CO_2 adsorption amount at 100 kPa. It was reported that simulated CO_2 adsorption isotherms at ∼25−30 °C[28,46] could not account for the hysteretic behavior, presumably because of a lack of structural information on the ZIF-7-I phase, and thus showed reversible adsorption/desorption behaviors. Figure S10 reveals that the simulated CO_2 adsorption isotherms followed the general trend of monotonic, smooth increase, and in particular, the result reported by Morris et al.[46] was in good agreement with that of ZIF-7-S at 30 °C shown in Figure 5a2.

Despite the similarities between the simulated adsorption data for ZIF-7[46] and the experimental data for ZIF-7-S in this study, the activation process for the experimental counterpart[46] was apparently not appropriately conducted because the resulting XRD pattern was identical to the simulated ZIF-7 XRD pattern; this indicated that the occluded molecules were not yet fully removed, as discussed from the results in Figure 3. Nevertheless, hysteretic behavior was observed in the experimental CO_2 adsorption isotherm of ZIF-7 in that study.[46] This also addresses the importance of ZIF-7 handling for an accurate understanding of its intrinsic properties (here, CO_2 adsorption isotherms) and for its appropriate use in applications. Figures S11 and S12 indicate that the environment during heat treatment was irrelevant to ZIF-7 activation, as reflected by the almost identical XRD patterns and CO_2 adsorption isotherms at 30 °C for heat-treated ZIF-7-x (x = S, D, R) under air and vacuum conditions.

With the discrepant, unique CO_2 adsorption isotherms, we turned to NMR techniques in an attempt to assess the possible defects inside ZIF-7s. Although ^{67}Zn NMR spectra would be useful for this purpose, the low content of Zn inside ZIF-7 and the low natural isotopic abundance and small magnetogyric ratio of ^{67}Zn make it challenging to obtain ^{67}Zn NMR spectra of ZIF-7.[47] Alternatively, the ^{13}C cross-polarization/magic-angle-spinning (CP/MAS) NMR spectra of as-synthesized ZIF-7s (ZIF-7-x; x = S, D, R) and heat-treated ZIF-7s (ZIF-7-x_200_2d) were obtained (Figure S13). For all three samples, the ^{13}C CP/MAS NMR spectra also evidenced the presence of DMF, as observed for their FT-IR spectra (Figure S2). After heat treatments at 200 °C for 2 days, it appeared that DMF was almost completely removed from the ZIF-7 structure. There was no marked difference among the ^{13}C CP/MAS NMR spectra of ZIF-7-x_200_2d, but we noticed that the spectra corresponding to the carbon positions 3 and 4 in the benzimidazolate (Figure S13) had multiple sharp peaks and were comparable for ZIF-7-D and -R, while for ZIF-7-S the counterparts were rather smeared out. This can be understood by the possible presence of disordered structures near the outer surface for the smallest ZIF-7-S. The disordered structure could be more flexible than the core ZIF-7 structure, interacting with guest molecules (here CO_2) and favoring their facile adsorption/diffusion inside. This flexibility, which would be expected to decrease at lower temperatures, is also supported by the increased degree of the hysteresis in ZIF-7 at low temperatures (0 and 15 °C) (Figure 5a2). On the contrary, the rigid structures in the larger ZIF-7-D and -R would not provide the same degree of structural flexibility, and thus, a higher CO_2 pressure would be required to induce the preferred interaction that leads to its adsorption/diffusion inside ZIF-7s. Proposed schematics for the structures of ZIF-7-S and ZIF-7-D and -R are illustrated in Scheme S1 in the Supporting Information.

The remarkable discrepancy in the CO_2 adsorption isotherms of the three ZIF-7s in Figure 5a2−c2 can be understood by the above-mentioned disordered structure in ZIF-7-S, as its degree is generally increased with decreasing particle size. The agreement between the isotherm for ZIF-7-S and the simulated counterpart[46] (Figure S10) possibly indicates that although ZIF-7-S was transformed into the ZIF-7-S-I phase after guest molecule removal, the structure of ZIF-7-S-I was still close to that of the original ZIF-7-S and the transport resistance near and on the outer surface was not pronounced in the ZIF-7-S and ZIF-7-S-I phases. Furthermore, the isosteric heats of CO_2 adsorption calculated from the CO_2 adsorption points at

30−75 °C for ZIF-7-S in Figure 5a2 were ∼32−34 kJ·mol^{-1} (Figure S14), which were very close to the calculated binding energies of 29.6 or 31.8 kJ·mol^{-1} in preferential CO_2 adsorption sites.[46] This remarkable agreement also supports the plausible similarity between the ZIF-7-S and ZIF-7-S-I structures.

In order to obtain ZIF-7 with ideal intrinsic properties, it must undergo appropriate activation, mainly by heat treatment. In this study, the complete removal of guest molecules (mainly DMF) from ZIF-7 by conducting the heat treatment at ∼200 °C allowed for a fully opened pore structure accompanied by the inevitable structural transition of ZIF-7 to the ZIF-7-I phase (Figure 2a). With respect to membrane-based H_2/CO_2 separation, one of the promising candidates for the utilization of ZIF-7 was tested up to 220 °C in the literature,[27] and it was found that the structure of the as-synthesized or dried ZIF-7 membranes could be changed to a mixed phase containing ZIF-7 and the unknown phase (i.e., ZIF-7-I) depending on the exposure time and environment. For example, above a CO_2 partial pressure of ∼60 kPa at 30 °C, the ZIF-7 phase would be recovered;[28] however, at a higher temperature, the 60 kPa partial pressure would not be enough to maintain the original ZIF-7 phase. Although the ZIF-7 phase would be preserved near the membrane surface, the gradual structural change along the membrane thickness due to the monotonically decreasing fugacity is likely to occur. Accordingly, H_2/CO_2 separations would not be determined by the intrinsic molecular sieving of ZIF-7, although the low CO_2 adsorption capacity for ZIF-7-D and -R is beneficial in improving H_2 separations via a reduction in the CO_2 permeation rate. On the contrary, the reversible CO_2 adsorption behavior of ZIF-7-S at ∼30−75 °C is rather desirable for CO_2/N_2 separations in the postcombustion process compared with ZIF-7-D and -R.

Importantly, the hysteretic CO_2 adsorption behavior shown in Figure 5b2,c2 demonstrates the difficulty in desorbing the permeating molecules in ZIF-7 membrane constituents, probably resulting in the unexpected permeation results and, accordingly, separation performance. This in turn requires a rigorous analysis of the effects of hysteretic adsorption/desorption behaviors on the permeation flux. In particular, the CO_2 adsorption points for ZIF-7-D and -R were comparable, while the desorption points differed considerably; lower pressures were required to desorb CO_2 molecules for ZIF-7-D, indicating the greater difficulty in removing preadsorbed CO_2. In view of the fact that the size of ZIF-7-D is smaller than that (in either the radial or longitudinal direction) of ZIF-7-R, the pronounced irreversible adsorption behavior for ZIF-7-D, as reflected by the wider hysteresis in Figure 5b2, suggested that the CO_2 desorption behavior was not related to the particle size because smaller particles would provide more flexible structures, as shown for ZIF-7-S. Since the XRD and NMR data revealed that ZIF-7-D and -R shared almost identical ZIF-7 structures (Figures 2 and S13), the adsorption/desorption behavior was likely determined by an additional resistance on the outer surface (often called a surface barrier or resistance).[36,48] Because the discrepant behavior was observed only for desorption, not adsorption, it can be attributed to a distinctive transport resistance for desorption processes. One plausible scenario is that the preadsorbed CO_2 molecules in ZIF-7-D might experience more difficulty while desorbing as a result of inhibition by other CO_2 molecules adsorbed on and/or near the outer surface, as supported by the ∼6 times higher surface-to-volume ratio for ZIF-7-D than for ZIF-7-R. This rather suggested the dependence of the hysteric behavior on the particle size of ZIF-7s.

When the discrepant adsorption−desorption behaviors in all of the ZIF-7s as shown in Figure 5a2−c2 are taken into account, the CO_2 adsorption behaviors, if extracted or estimated from a direct measurement via the ZIF-7 membranes, will be desirable for predicting and deciphering CO_2 permeation fluxes. If the discrepancy were to originate from the outer surface of ZIF-7, a molecular transport mechanism on the membrane surface and interface with a support, reflected by either surface resistance[49−51] or gate-opening behavior,[12,32,52,53] should be appropriately taken into account. In view of the coupled effects of adsorption and diffusion on membrane permeation, molecular simulations of the adsorption/desorption behaviors and diffusion inside ZIF-7 as well as permeation modeling for ZIF-7 membranes are important for appropriately representing the permeation flux and thus the separation performance.

4. CONCLUSION

In summary, we have synthesized three types of ZIF-7 particles (ZIF-7-S, -D, and -R) that differ in both shape and size. Heat treatments of all three ZIF-7 materials at 200 °C under air resulted in the appearance of new XRD peaks in addition to those of the original ZIF-7 phase (i.e., corresponding to the ZIF-7-I phase). Heat treatment at a higher temperature (above 200 °C) under air produced a gradual change in the ZIF-7 structure eventually toward the zinc oxide phase. The phase transition could apparently be regarded as a kinetically limited process, as reflected by the delayed process rate in the largest ZIF-7-R. In addition, we found that the guest molecules in the three ZIF-7s were mainly DMF solvent molecules, not water molecules, unlike the well-known result in the literature. This points to the importance of the accurate understanding of ZIF-7s (obtained by different synthetic routes and prepared by various post-treatments) for appropriate use.

In contrast, thermal treatments in inert environments did not result in the complete phase transition to zinc oxide up to ∼500 °C, after which structural collapse occurred instead. The high thermal stability in inert environments revealed the strong interaction between the ZIF-7 components. In addition, we found that when the guest molecules (water and DMF) were removed, new XRD peaks corresponding to ZIF-7-I appeared, indicating thermal activation accompanied by an inevitable structural change.

Finally, the distinct CO_2 adsorption isotherms of the three types of ZIF-7 suggested that the adsorption−desorption behavior was strongly correlated to the synthesis protocol and thus that a disordered structure near the surface (usually pronounced for smaller particles) and/or a surface barrier (requiring study at the fundamental level) on the outer surface plausibly exists, affirming the importance of the rigorous analysis of ZIF-7 structures for reliable use in desired applications. Currently, we are attempting to interpret the structural changes in ZIF-7 due to the desorption of guest molecules from the ZIF-7 framework crystallographically with the aim of elucidating the effects of structural changes on the resulting adsorption properties, mainly for effective CO_2 separations.

dx.doi.org/10.1021/ja5016298 | J. Am. Chem. Soc. 2014, 136, 7961−7971

■ ASSOCIATED CONTENT

Supporting Information

SEM, XRD, FT-IR, and NMR results for heat-treated ZIF-7 particles under various conditions; SEM images, XRD patterns, N_2 physisorption data, and CO_2 adsorption isotherms for particles synthesized in methanol or ethanol media; simulated CO_2 adsorption isotherms for ZIF-7; and isosteric heat of CO_2 adsorption for ZIF-7-S. This material is available free of charge via the Internet at http://pubs.acs.org.

■ AUTHOR INFORMATION

Corresponding Author

jungkyu_choi@korea.ac.kr

Notes

The authors declare no competing financial interest.

■ ACKNOWLEDGMENTS

This work was supported by the Korea CCS R&D Center (KCRC) and by the National Research Foundation (NRF) (2011-0031318 & 2012-2012R1A1A1042450). All grants were funded by the Government of Korea (Ministry of Science, ICT & Future Planning). SEM and XRD experiments were conducted at the Korea University Engineering Laboratory Center, while TGA, 13C CP/MAS NMR, and programmed XRD analyses were carried out at the Korea Institute of Science and Technology (KIST), the Korea Basic Science Institute (KBSI), and the Korea Electronics Technology Institute (KETI), respectively.

■ REFERENCES

(1) Phan, A.; Doonan, C. J.; Uribe-Romo, F. J.; Knobler, C. B.; O'Keeffe, M.; Yaghi, O. M. *Acc. Chem. Res.* **2010**, *43*, 58.

(2) Shah, M.; McCarthy, M. C.; Sachdeva, S.; Lee, A. K.; Jeong, H. K. *Ind. Eng. Chem. Res.* **2012**, *51*, 2179.

(3) Banerjee, R.; Phan, A.; Wang, B.; Knobler, C.; Furukawa, H.; O'Keeffe, M.; Yaghi, O. M. *Science* **2008**, *319*, 939.

(4) Park, K. S.; Ni, Z.; Cote, A. P.; Choi, J. Y.; Huang, R. D.; Uribe-Romo, F. J.; Chae, H. K.; O'Keeffe, M.; Yaghi, O. M. *Proc. Natl. Acad. Sci. U.S.A.* **2006**, *103*, 10186.

(5) Hwang, Y.; Sohn, H.; Phan, A.; Yaghi, O. M.; Candler, R. N. *Nano Lett.* **2013**, *13*, 5271.

(6) Lu, G.; Farha, O. K.; Zhang, W. N.; Huo, F. W.; Hupp, J. T. *Adv. Mater.* **2012**, *24*, 3970.

(7) Karagiaridi, O.; Lalonde, M. B.; Bury, W.; Sarjeant, A. A.; Farha, O. K.; Hupp, J. T. *J. Am. Chem. Soc.* **2012**, *134*, 18790.

(8) Jiang, H. L.; Liu, B.; Akita, T.; Haruta, M.; Sakurai, H.; Xu, Q. *J. Am. Chem. Soc.* **2009**, *131*, 11302.

(9) Kuo, C. H.; Tang, Y.; Chou, L. Y.; Sneed, B. T.; Brodsky, C. N.; Zhao, Z. P.; Tsung, C. K. *J. Am. Chem. Soc.* **2012**, *134*, 14345.

(10) Lu, G.; Li, S. Z.; Guo, Z.; Farha, O. K.; Hauser, B. G.; Qi, X. Y.; Wang, Y.; Wang, X.; Han, S. Y.; Liu, X. G.; DuChene, J. S.; Zhang, H.; Zhang, Q. C.; Chen, X. D.; Ma, J.; Loo, S. C. J.; Wei, W. D.; Yang, Y. H.; Hupp, J. T.; Huo, F. W. *Nat. Chem.* **2012**, *4*, 310.

(11) Alkordi, M. H.; Liu, Y. L.; Larsen, R. W.; Eubank, J. F.; Eddaoudi, M. *J. Am. Chem. Soc.* **2008**, *130*, 12639.

(12) Gücüyener, C.; van den Bergh, J.; Gascon, J.; Kapteijn, F. *J. Am. Chem. Soc.* **2010**, *132*, 17704.

(13) Li, J. R.; Ma, Y. G.; McCarthy, M. C.; Sculley, J.; Yu, J. M.; Jeong, H. K.; Balbuena, P. B.; Zhou, H. C. *Coord. Chem. Rev.* **2011**, *255*, 1791.

(14) Li, T.; Pan, Y. C.; Peinemann, K. V.; Lai, Z. P. *J. Membr. Sci.* **2013**, *425*, 235.

(15) Kang, C. H.; Lin, Y. F.; Huang, Y. S.; Tung, K. L.; Chang, K. S.; Chen, J. T.; Hung, W. S.; Lee, K. R.; Lai, J. Y. *J. Membr. Sci.* **2013**, *438*, 105.

(16) Zhang, L. L.; Hu, Z. Q.; Jiang, J. W. *J. Phys. Chem. C* **2012**, *116*, 19268.

(17) Yang, T. X.; Xiao, Y. C.; Chung, T. S. *Energy Environ. Sci.* **2011**, *4*, 4171.

(18) Bux, H.; Feldhoff, A.; Cravillon, J.; Wiebcke, M.; Li, Y. S.; Caro, J. *Chem. Mater.* **2011**, *23*, 2262.

(19) Pan, Y. C.; Liu, Y. Y.; Zeng, G. F.; Zhao, L.; Lai, Z. P. *Chem. Commun.* **2011**, *47*, 2071.

(20) Li, Y. S.; Liang, F. Y.; Bux, H.; Feldhoff, A.; Yang, W. S.; Caro, J. *Angew. Chem., Int. Ed.* **2010**, *49*, 548.

(21) Kwon, H. T.; Jeong, H. K. *J. Am. Chem. Soc.* **2013**, *135*, 10763.

(22) Huang, A. S.; Dou, W.; Caro, J. *J. Am. Chem. Soc.* **2010**, *132*, 15562.

(23) Sun, C. Y.; Qin, C.; Wang, X. L.; Yang, G. S.; Shao, K. Z.; Lan, Y. Q.; Su, Z. M.; Huang, P.; Wang, C. G.; Wang, E. B. *Dalton Trans.* **2012**, *41*, 6906.

(24) Qin, J. S.; Du, D. Y.; Li, W. L.; Zhang, J. P.; Li, S. L.; Su, Z. M.; Wang, X. L.; Xu, Q.; Shao, K. Z.; Lan, Y. Q. *Chem. Sci.* **2012**, *3*, 2114.

(25) Hu, Z. Q.; Chen, Y. F. *Mol. Simul.* **2012**, *38*, 830.

(26) Thornton, A. W.; Dubbeldam, D.; Liu, M. S.; Ladewig, B. P.; Hill, A. J.; Hill, M. R. *Energy Environ. Sci.* **2012**, *5*, 7637.

(27) Li, Y. S.; Liang, F. Y.; Bux, H. G.; Yang, W. S.; Caro, J. *J. Membr. Sci.* **2010**, *354*, 48.

(28) Aguado, S.; Bergeret, G.; Titus, M. P.; Moizan, V.; Nieto-Draghi, C.; Bats, N.; Farrusseng, D. *New J. Chem.* **2011**, *35*, 546.

(29) He, M.; Yao, J. F.; Li, L. X.; Wang, K.; Chen, F. Y.; Wang, H. T. *ChemPlusChem* **2013**, *78*, 1222.

(30) Peralta, D.; Chaplais, G.; Simon-Masseron, A.; Barthelet, K.; Chizallet, C.; Quoineaud, A. A.; Pirngruber, G. D. *J. Am. Chem. Soc.* **2012**, *134*, 8115.

(31) Zhang, L. L.; Hu, Z. Q.; Jiang, J. W. *J. Am. Chem. Soc.* **2013**, *135*, 3722.

(32) Fairen-Jimenez, D.; Moggach, S. A.; Wharmby, M. T.; Wright, P. A.; Parsons, S.; Düren, T. *J. Am. Chem. Soc.* **2011**, *133*, 8900.

(33) Dong, X. L.; Huang, K.; Liu, S. N.; Ren, R. F.; Jin, W. Q.; Lin, Y. S. *J. Mater. Chem.* **2012**, *22*, 19222.

(34) Thompson, J. A.; Blad, C. R.; Brunelli, N. A.; Lydon, M. E.; Lively, R. P.; Jones, C. W.; Nair, S. *Chem. Mater.* **2012**, *24*, 1930.

(35) Xie, J.; Yan, N.; Liu, F.; Qu, Z.; Yang, S.; Liu, P. *Front. Environ. Sci. Eng.* **2014**, *8*, 162.

(36) Kärger, J.; Ruthven, D. M. *Diffusion in Zeolites and Other Microporous Solids*; John Wiley & Sons: New York, 1992.

(37) Kortunov, P. V.; Heinke, L.; Arnold, M.; Nedellec, Y.; Jones, D. J.; Caro, J.; Karger, J. *J. Am. Chem. Soc.* **2007**, *129*, 8041.

(38) Tzoulaki, D.; Heinke, L.; Lim, H.; Li, J.; Olson, D.; Caro, J.; Krishna, R.; Chmelik, C.; Karger, J. *Angew. Chem., Int. Ed.* **2009**, *48*, 3525.

(39) Zhang, L.; Chmelik, C.; van Laak, A. N. C.; Karger, J.; de Jongh, P. E.; de Jong, K. P. *Chem. Commun.* **2009**, 6424.

(40) Reyes, S. C.; Santiesteban, J. G.; Ni, Z.; Paur, C. S.; Kortunov, P.; Zengel, J.; Deckman, H. W. (ExxonMobil Research and Engineering Co., USA). US 2009-321751, 2009.

(41) Merkel, T. C.; Lin, H. Q.; Wei, X. T.; Baker, R. *J. Membr. Sci.* **2010**, *359*, 126.

(42) Zhang, P.; Sun, F.; Xiang, Z. H.; Shen, Z. G.; Yun, J.; Cao, D. P. *Energy Environ. Sci.* **2014**, *7*, 442.

(43) Li, Y. S.; Bux, H.; Feldhoff, A.; Li, G. L.; Yang, W. S.; Caro, J. *Adv. Mater.* **2010**, *22*, 3322.

(44) Gustafsson, M.; Zou, X. D. *J. Porous Mater.* **2013**, *20*, 55.

(45) van den Bergh, J.; Gücüyener, C.; Pidko, E. A.; Hensen, E. J. M.; Gascon, J.; Kapteijn, F. *Chem.—Eur. J.* **2011**, *17*, 8832.

(46) Morris, W.; He, N.; Ray, K. G.; Klonowski, P.; Furukawa, H.; Daniels, I. N.; Houndonougbo, Y. A.; Asta, M.; Yaghi, O. M.; Laird, B. B. *J. Phys. Chem. C* **2012**, *116*, 24084.

(47) Sutrisno, A.; Terskikh, V. V.; Shi, Q.; Song, Z. W.; Dong, J. X.; Ding, S. Y.; Wang, W.; Provost, B. R.; Daff, T. D.; Woo, T. K.; Huang, Y. N. *Chem.—Eur. J.* **2012**, *18*, 12251.

(48) Teixeira, A. R.; Chang, C. C.; Coogan, T.; Kendall, R.; Fan, W.; Dauenhauer, P. J. *J. Phys. Chem. C* **2013**, *117*, 25545.

(49) Bux, H.; Chmelik, C.; Krishna, R.; Caro, J. *J. Membr. Sci.* **2011**, *369*, 284.
(50) Reitmeier, S. J.; Gobin, O. C.; Jentys, A.; Lercher, J. A. *Angew. Chem., Int. Ed.* **2009**, *48*, 533.
(51) Hibbe, F.; Chmelik, C.; Heinke, L.; Pramanik, S.; Li, J.; Ruthven, D. M.; Tzoulaki, D.; Karger, J. *J. Am. Chem. Soc.* **2011**, *133*, 2804.
(52) Kondo, A.; Noguchi, H.; Ohnishi, S.; Kajiro, H.; Tohdoh, A.; Hattori, Y.; Xu, W. C.; Tanaka, H.; Kanoh, H.; Kaneko, K. *Nano Lett.* **2006**, *6*, 2581.
(53) Seo, J.; Matsuda, R.; Sakamoto, H.; Bonneau, C.; Kitagawa, S. *J. Am. Chem. Soc.* **2009**, *131*, 12792.

dx.doi.org/10.1021/ja5016298 | *J. Am. Chem. Soc.* 2014, 136, 7961−7971